Caught in the Act: The 1.5 Å Resolution Crystal Structures of the HIV-1 Protease and the I54V Mutant Reveal a Tetrahedral Reaction Intermediate†

Andrey Y. Kovalevsky,‡ Alexander A. Chumanevich,‡ Fengling Liu,‡ John M. Louis,§ and Irene T. Weber*,‡,||

Departments of Biology and Chemistry, Molecular Basis of Disease Program, Georgia State University, Atlanta, Georgia 30303, and Laboratory of Chemical Physics, National Institute of Diabetes and Digestive and Kidney Diseases, National Institutes of Health, Bethesda, Maryland 20892

Received May 1, 2007; Revised Manuscript Received October 22, 2007

ABSTRACT: HIV-1 protease (PR) is the target for several important antiviral drugs used in AIDS therapy. The drugs bind inside the active site cavity of PR where normally the viral polyprotein substrate is bound and hydrolyzed. We report two high-resolution crystal structures of wild-type PR (PR_{WT}) and the multi-drug-resistant variant with the I54V mutation (PR_{I54V}) in complex with a peptide at 1.46 and 1.50 Å resolution, respectively. The peptide forms a *gem*-diol tetrahedral reaction intermediate (TI) in the crystal structures. Distinctive interactions are observed for the TI binding in the active site cavity of PR_{WT} and PR_{I54V}. The mutant PR_{I54V}/TI complex has lost water-mediated hydrogen bond interactions with the amides of Ile50 and Ile50′ in the flap. Hence, the structures provide insight into the mechanism of drug resistance arising from this mutation. The structures also illustrate an intermediate state in the hydrolysis reaction. One of the *gem*-diol hydroxide groups in the PR_{WT} complex forms a very short (2.3 Å) hydrogen bond with the outer carboxylate oxygen of Asp25. Quantum chemical calculations based on this TI structure are consistent with protonation of the inner carboxylate oxygen of Asp25′, in contrast to several theoretical studies. These TI complexes and quantum calculations are discussed in relation to the chemical mechanism of the peptide bond hydrolysis catalyzed by PR.

HIV-1 protease (PR)[1] is an indispensable viral enzyme that cleaves the viral Gag and Gag-Pol polyproteins into the individual enzymes and structural proteins during the late stages of the viral life cycle (*1*). Therefore, disruption of the PR activity results in an immature viral particle unable to infect other cells. This knowledge was employed in the discovery of PR inhibitors that, in the past decade, have revolutionized the treatment of AIDS (*2*, *3*). However, HIV-1 quickly mutates to confer resistance to the administered drugs, leading to failure of the treatment regimen in many cases (*4*). Consequently, the molecular mechanisms of PR inhibition and activity must be comprehended to develop new strategies to overcome drug resistance.

The active PR is a homodimer containing 99 amino acid residues in each subunit. As in other aspartic proteases, the active site is composed of two conserved triads with the sequence Asp-Thr-Gly. The PR dimer forms a large active site cavity between the two subunits, where an inhibitor or substrate can bind. Many crystal structures of PR/inhibitor complexes have revealed how various inhibitors bind in the active site cavity of the wild-type PR or its mutants (*5*−*11*). Several drug-resistant mutations alter residues that interact with inhibitor in the active site cavity and reduce the affinity for the inhibitor. However, other resistant mutations, such as I54V, alter residues that lack specific contacts with inhibitors and have more indirect effects. I54V is a multi-drug-resistant mutation that contributes resistance to all clinically available PR inhibitors (*4*). This mutation alone does not lead to resistance, but it appears in combination with other drug-resistant mutations. Moreover, it is found in more than 30% of patients treated with more than one PR inhibitor. Drug-resistant PR must retain the ability to bind and hydrolyze substrates, despite the altered interactions with inhibitors. However, the active PR will readily hydrolyze a peptide substrate, which generally precludes crystallization and structural analysis of a PR/substrate complex. This obstacle has been overcome by either chemically changing the scissile peptide bond to a nonhydrolyzable group (e.g., carbonyl is reduced to a methylene group) (*12*−*14*) or mutating the catalytic aspartate of PR to asparagine (*15*−*17*). In the former case, the complex will contain a substrate analogue inhibitor, while the latter modification produces an inactive PR mutant. Although these structures have provided insights into the specificity and mode of substrate binding in the PR active site cavity, they do not fully represent the cleavable substrate bound to the catalytic aspartates.

† This research was supported in part by the Molecular Basis of Disease Program, the Georgia Research Alliance, the Georgia Cancer Coalition, National Institutes of Health Grant GM62920, and the Intramural Research Program of the NIDDK, NIH. Use of the Advanced Photon Source was supported by the U.S. Department of Energy, Office of Science, Office of Basic Energy Sciences, under Contract No. DE-AC02-06CH11357.

* To whom correspondence should be addressed. Phone: (404) 413-5411. Fax: (404) 413-5301. E-mail: iweber@gsu.edu.

‡ Department of Biology, Georgia State University.

§ Department of Chemistry, Georgia State University.

|| National Institutes of Health.

[1] Abbreviations: HIV-1, human immunodeficiency virus type 1; PR, HIV-1 protease; TI, *gem*-diol−amine tetrahedral intermediate.

10.1021/bi700822g CCC: $37.00
Published on Web 12/04/2007

The reaction mechanism of PR-catalyzed hydrolysis of peptides has been studied experimentally and theoretically (see, for example, a review by Brik and Wong (*18*)). The reaction is considered to proceed via formation of a metastable tetrahedral *gem*-diol−amine (or simply *gem*-diol) intermediate, in agreement with ^{18}O-exchange NMR experiments (*19*). The HIV-1 PR active site contains two Asp25 residues with ∼2.5−2.7 Å separation between the inner carboxylate oxygen atoms, while one of the oxygens is assumed to be protonated. However, no agreement has been reached on the exact position of the proton. Several theoretical studies of the mechanism have concluded that the outer oxygen of Asp25 is protonated (*20*−*22*), while others proposed protonation of the inner oxygen (*23*, *24*).

Ideally, a reactive substrate would be cocrystallized with the active HIV-1 PR to trap a reaction intermediate. Kumar et al. (*25*). have reported the crystal structure of HIV-1 PR in complex with the tetrahedral intermediate of the substrate HKARVL*p(NO_2)FEAL^{n}S (where the asterisk denotes the cleavage site, p(NO_2)F is *p*-nitrophenylalanine, and L^n is norleucine) at 2.03 Å resolution. The PR was constructed as a C95M/C95′A heterodimeric double mutant with a −GGSSG− linker covalently connecting the two monomers between residues 99 and 1′. However, the geometric accuracy may be limited due to the resolution and presence of disorder from two orientations of the substrate.

We report two high-resolution crystal structures of wild-type PR (PR_{WT}) and the multi-drug-resistant variant with the I54V mutation (PR_{I54V}) in complex with a short peptide at 1.46 and 1.50 Å resolution, respectively. The peptide forms a single conformation of the *gem*-diol tetrahedral reaction intermediate (TI) in the crystal structures. Distinctive interactions are observed for the TI binding in the active site cavity of PR_{WT} and PR_{I54V}. Hence, the structures provide insight into the changes in PR activity arising from this mutation. Additionally, the TI complexes and associated quantum chemical calculations are discussed in relation to the chemical mechanism of the peptide hydrolysis catalyzed by PR.

EXPERIMENTAL PROCEDURES

Preparation of HIV-1 PR_{WT} and PR_{I54V}, Purification, and Crystallization. A pentasubstituted HIV-1 PR clone (Q7K, L33I, L63I, C67A, C95A) was used as the wild-type template to introduce the single mutation I54V, as described elsewhere (*26*). The PR_{WT} and PR_{I54V} mutant were expressed in *Escherichia coli* and purified from the inclusion bodies by the reported procedure (*27*).

The crystals of PR_{WT}/TI and PR_{I54V}/TI complexes were grown by the hanging-drop vapor diffusion method. In the case of PR_{WT}/TI a 1 mL reservoir solution contained 50 mM sodium phosphate/100 mM sodium citrate buffer (pH 6.0), 10% NaCl (w/w), and 2.5% (v/v) glycerol. For PR_{I54V}/TI, the reservoir had 12.5 mM sodium phosphate/50 mM sodium citrate buffer (pH 6.0), 8% NaCl, and 10% glycerol. The concentrations of the PR_{WT} and PR_{I54V} mutant were 1.2 and 2.5 mg/mL, respectively. Platelike crystals appeared in 1−2 weeks and reached a usable size of 0.2 × 0.2 × 0.05 mm within 4 weeks in both cases.

X-ray Data Collection and Refinement. Crystals were cryoprotected with the reservoir solution containing 25% (v/v) glycerol, mounted on a nylon loop, and flash-frozen in liquid nitrogen. X-ray diffraction data were collected on the SER-CAT (22ID) beamline of the Advanced Photon Source, Argonne National Laboratory, at 100 K using 1.0 Å (PR_{WT}/TI) and 0.8 Å (PR_{I54V}/TI) wavelengths. The data were processed with HKL2000 (*28*). The CCP4i suite of programs (*29*, *30*) was used to obtain a molecular replacement solution (program Phaser) using the wild-type PR structure complexed with the inhibitor darunavir (DRV) (PDB 2IEN) (*31*) as the initial model. The structures were refined using SHELX97 (*32*) and refitted with the O10 (*33*) program. Alternate conformations were modeled for the PR residues when obvious in the electron density maps. Anisotropic atomic displacement parameters (*B* factors) were refined for all atoms including solvent molecules. Hydrogen atoms were added to the PR atoms at the final stages of the refinement. The identity of the ions and other solvent molecules in the crystallization solutions was deduced from the shape and peak height of the $2F_o - F_c$ and $F_o - F_c$ electron density, the potential hydrogen bond interactions, and the interatomic distances. The PR_{WT}/TI crystal structure was refined with 1 sodium cation, 3 chloride anions, 1 glycerol molecule, and 172 water molecules including partial occupancy sites. The PR_{I54V}/TI structure included 1 sodium cation, 3 chloride anions, and 189 water molecules including partial occupancy sites. The TI sequence was estimated from the shape of the electron density to be AIL*VQN (where the asterisk denotes the *gem*-diol position) although the termini are partially disordered. The TI peptide occupancy was refined in SHELXL using a least-squares method to 60% in both wild-type and I54V mutant structures. The other 40% were presumed to be the products of the hydrolysis reaction that were released from the active site cavity into the bulk water. The figures were made with PyMol (*34*).

Mass Spectrometry. Samples from the stock solution of purified HIV-1 protease and freshly grown crystals were analyzed by SDS−PAGE, MALDI-TOF analysis on a Voyager-DE instrument (PerSeptive Biosystems), and N-terminal sequencing. Mass peaks were observed in the dissolved crystals for the HIV-1 protease at m/z 10720 (+1) and 9363 (+2). Additional major peaks were observed at m/z 2602, 1423, 657, and 446; however, the smaller molecules could not be positively identified by further post source decay analysis. SDS−PAGE analysis of the stock solution used for growing the crystals showed the protease and two smaller proteins. N-terminal sequencing confirmed the presence of the full-length protease and two of its fragments starting at residues I(33)EEMSL and T(74)-VLVPGT.

DFT Quantum Chemical Calculations. All calculations were performed with the GAUSSIAN03 package (*35*) by using density functional theory (DFT) with the hybrid functional B3LYP. A triple-ζ 6-311++G** basis set was used for all atoms. All molecular geometries were optimized without symmetry restrictions. The positions of most heavy atoms were obtained from the X-ray analysis data and were fixed during the entire geometry optimization, while the positions of all hydrogen atoms were free to optimize. In addition, C−O distances of side chain carboxylic moieties were included in the geometry optimization to account for the protonation of these residues, which is invisible in the crystal structures. The convergence criteria were 10^{-6} au for the density matrix, 4.5×10^{-4} au Å^{-1} for the gradients, and

Table 1: Data Collection and Refinement Statistics for PR_{WT} and PR_{I54V} in Complex with the *gem*-Diol Tetrahedral Intermediate

	PR_{WT}	PR_{I54V}
Data Collection		
space group	P 2_1 2_1 2	P 2_1 2_1 2
unit cell dimensions, *a*, *b*, *c* (Å)	58.30, 86.12, 46.31	58.44, 86.02, 46.31
resolution range (Å)	50−1.46 (1.50−1.46)[a]	50−1.50 (1.55−1.50)
no. of unique reflns [obsd with $I > 2\sigma(I)$]	40 494 [32 850]	37 411 [30 352]
$I/\sigma(I)$	14.0 (2.0)	26.1 (2.2)
R_{merge} (%)	10.3 (48.1)	6.4 (47.2)
completeness (%)	97.9 (87.2)	98.2 (85.8)
Refinement		
data range for refinement (Å)	10−1.46	10−1.50
R_{work} (%)	15.5	15.6
R_{free} (%) (5% of reflns randomly)	21.2	21.9
no. of solvent molecules	177	193
RMS deviation from ideality		
bonds (Å)	0.011	0.011
angles (Å)	0.030	0.032
average *B* factors (Å^2)		
main chain	15.4	15.4
side chain	25.9	25.8
tetrahedral intermediate	26.7	36.0
solvent	37.2	40.2
occupancy of TI (%)	60	60

[a] The numbers in parentheses are given for the highest resolution shell.

1.8×10^{-3} Å for the displacements. All calculations were spin-restricted. The computations were run on the IBM System p5 575 with Power5+ processors at Georgia State University. System p5 runs the AIX 5.3 operating system using a 64-bit architecture. There are eight symmetric multiprocessor (SMP) nodes, each with eight dual-core 1.9 GHz processors for a total of 128 CPUs with 256 GB of total memory. A pSeries high-performance switch connects the nodes.

RESULTS

Crystallographic Analysis. The crystal structures of PR_{WT}/TI and PR_{I54V}/TI were solved in the space group $P2_12_12$ as summarized in Table 1. The asymmetric units contain the PR dimer, and the residues in the two subunits are labeled 1−99 and 1′−99′ (Figure 1). The crystals diffracted to a resolution of 1.46 Å for PR_{WT}/TI and 1.50 Å for PR_{I54V}/TI. The structures were refined with anisotropic *B* factors, solvent molecules, and hydrogen atoms. The final *R* factors are 15% for both structures. There was clear electron density for the majority of residues and solvent molecules in all the structures. The side chains of a few residues on the surface of the PR showed no density due to disorder over many possible positions.

There was clear electron density for the central four residues (P2−P2′) of the peptide TI in the wild type and the mutant PR structures (Figure 2). The TI adopts a single extended conformation in both complexes, and the initial amino acid sequence of AILVQN was estimated from the shape of the electron density. The density was partially disordered for the side chains of the terminal P3 and P3′

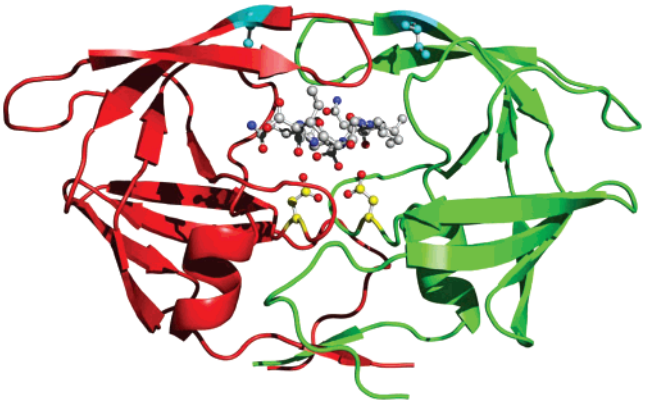

FIGURE 1: HIV-1 PR homodimer structure in cartoon representation showing the secondary structure. The tetrahedral intermediate (gray), Asp25 and Asp25′ (yellow), and site of mutation Ile54 to Val (cyan) are shown in ball-and-stick mode.

residues, and it is possible that the peptide is longer than the six residues visible in the structures. Also, the shape of the electron density is ambiguous for the P1′ and P2′ side chains. The density for P1′ can be fit by Val or Thr, and P2′ can be Glu or Gln. Further analysis of the PR solution by SDS−PAGE and N-terminal sequencing identified two fragments of the PR starting at residues 33 and 74. Therefore, the sequence of HIV-1 PR was examined for possible matches to the shape of the observed electron density for the P2−P2′ residues. The two possible peptides, residues 61−66 (QIIIEI) and 88−93 (NLLTQI), contain sites of autoproteolysis (*36*). Both peptides were evaluated by refinement in the crystal structures. The peptide QIIIEI was rejected, since the refinement performed poorly and the side chains of Ile-Ile were not a good fit for the Leu-Val-shaped side chain density at P1 and P1′. The other possible match of NLLTQI refined as well as the original estimated sequence, although it required one awkward fit of Leu for Ile-shaped density at P2. This fit can be achieved if the P2 Leu side chain has two alternate conformations. Although Thr is unusual at P1′, HIV-1 protease was shown to hydrolyze between Leu and Thr in a peptide representing a cleavage site of avian myeloblastosis virus protease (*37*). Hence, NLLTQI was selected as the best fit in the PR sequence for the TI peptide (Figure 2), although the presence of a different peptide cannot be ruled out.

Alternate conformations were modeled for residues in the two structures where clear electron density was present for the two conformations. There were 17 alternate conformations modeled in PR_{WT}/TI and 12 for PR_{I54V}/TI. Generally, the alternate conformations were observed for side chains of surface residues. The exceptions were the internal side chains of residues Val82 and Leu97 in both subunits of the two complexes, Ile84 in one subunit of PR_{WT}/TI, and Val32 in one subunit of PR_{I54V}/TI.

The high resolution of the diffraction data allowed modeling of two shells of solvent. The solvent was modeled with ~180 water molecules, ions, and other small molecules from the crystallization conditions; some of the solvent molecules had partial occupancy. The solvent ions were the sodium cation and chloride anion, while a glycerol molecule was refined in the PR_{WT}/TI structure.

Protease−TI Interactions. The tetrahedral intermediate was fitted with the sequence NLLTQI, where the *gem*-diol

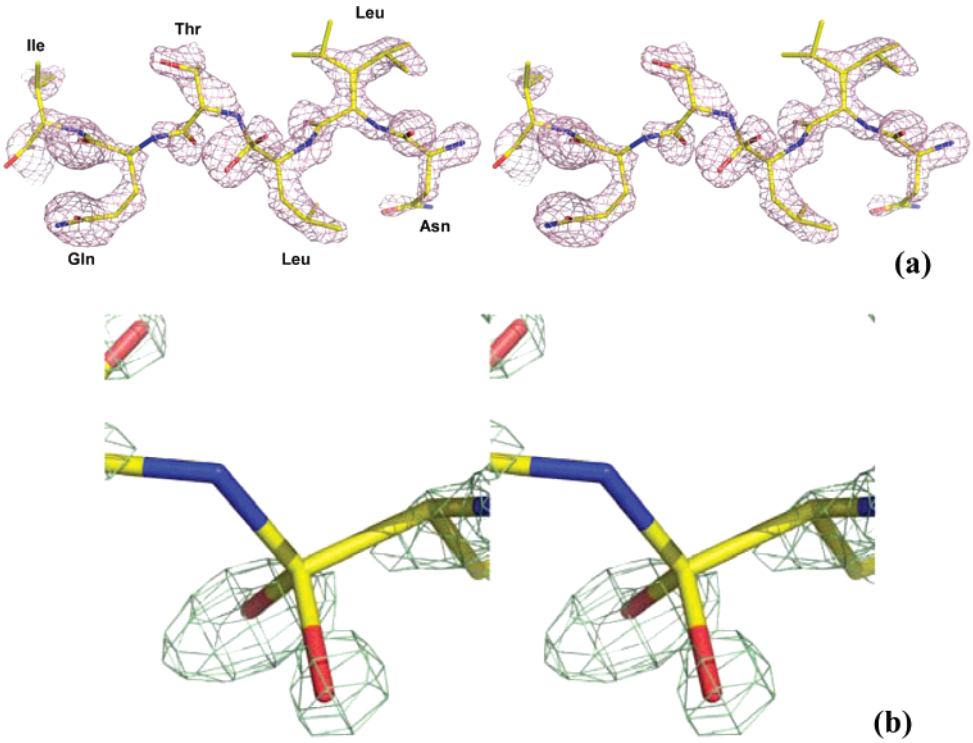

FIGURE 2: Stereo view of the omit electron density ($F_o - F_c$) for the tetrahedral intermediate in the PR_{WT}/TI structure. Contour levels are 2.2σ for **(**a**)** and 3.6σ for **(**b**)**. The higher contour level in **(**b**)** shows the positions of the TI hydroxyl oxygens.

lies between P1 Leu and P1′ Thr. The TI binds in the PR active site cavity by means of hydrogen bonds, hydrophilic C−H···O contacts, and hydrophobic CH···HC interactions very similar to those observed in PR complexes with peptide analogues containing P2′ Gln (*12*). Seven hydrogen bonds connect the main chain atoms of TI with residues Asp29, Gly48, Gly27′, Asp29′, and Gly48′ with distances of 2.9−3.1 Å (Figure 3a). The position and conformation of the TI are further stabilized by the well-known water-mediated hydrogen bonds that link the TI to the tips of the flaps. The flap water is equidistant from both carbonyl oxygens of P2 Leu and P1′ Thr residues of the TI (distances are 2.7 Å) and main chain amide nitrogens of Ile50 and Ile50′ (distances are 3.2 and 3.0 Å, respectively). The side chain of P2′ Gln forms additional N−H···O H bonds with the main (3.0 Å) and side (2.5 Å) chains of Asp30′ and the main chain amide of Asp29′ (3.1 Å). Other stabilizing interactions include C−H···O contacts (3.2−3.7 Å) that are observed mostly between main chains of the TI and PR_{WT}. Among those, (Gln_{TI})Cα···O═C(Gly48′) is the strongest interaction with a distance of 3.2 Å. The C−H···C−H hydrophobic TI−PR interactions have distances of around 4.0 Å. These interactions, in particular the hydrogen bond network, are well conserved throughout many PR/substrate analogue (*12*, *13*, *38*) and inactive PR/substrate (*15*−*17*) complexes. Consequently, it is expected that structural differences between the PR_{WT}/TI and PR/substrate (or substrate analogue) complexes will be confined to the active site residues and the scissile bond. The detailed geometry of the interactions between the catalytic aspartates and the TI *gem*-diol will be described in a later section.

Effects of the I54V Mutation on TI Binding and the PR Conformation. When the PR_{WT}/TI and PR_{I54V}/TI structures are superimposed, the root-mean-square deviation for the main chain atoms is 0.2 Å. Nevertheless, there are significant differences in the conformations of the PR residues that appear to be related to the single mutation I54V. Changes are seen in the interactions of Ile50 and Ile50′ with TI and around the mutated residue 54, which are associated with main chain shifts of about 0.5 Å for Ile50, Ile50′, Thr80, and Pro81.

The hydrogen bond network connecting TI with PR residues is mostly conserved between the two structures, with almost identical interatomic distances (Figure 3b). The P2′ Gln side chain has a similar number of hydrogen bonds, although rearranged, with the main chain atoms of Asp29′ and Asp30′. The major change is the weaker interactions of the TI with the flap residues in the mutant structure. The flap water in the PR_{I54V}/TI structure has only 60% occupancy and lacks hydrogen bonds with the main chain amides of Ile50 and Ile50′; the distances are elongated to 3.5 and 4.0 Å compared to 3.0 and 3.2 Å in the PR_{WT}/TI structure. Therefore, the flap water of the PR_{I54V}/TI complex retains only two hydrogen bonds, although their distances are similar to those observed in PR_{WT}/TI. The loss of the hydrogen bonds is associated with the ∼0.5 Å shift of Ile50 and Ile50′ away from the active site residues and the flap water (Figure 4).

In addition to the changes in atomic positions of Ile50 and Ile50′, the substitution of the bulky isoleucine 54 to the smaller valine results in significant shifts in the positions of neighboring residues Ile50′ and Thr80−Val82 (Figure 4). Ile50 and Ile50′ make favorable interactions with residues 47 and 54 and the 80's loop. In the PR_{WT}/TI structure, favorable hydrophobic interactions form between the side chains of Ile54 and Ile50′ with interatomic distances of ∼4.0 Å. Moreover, Cγ2 of Ile54 and the carbonyl of Ile50′ form a C−H···O interaction of 3.5 Å. The hydrophilic contact is maintained in the mutant structure due to the ∼0.6 Å shift of Ile50′, while the hydrophobic contacts are elongated to 4.4 Å (Figure 4). There is a concerted shift of Ile50′ and

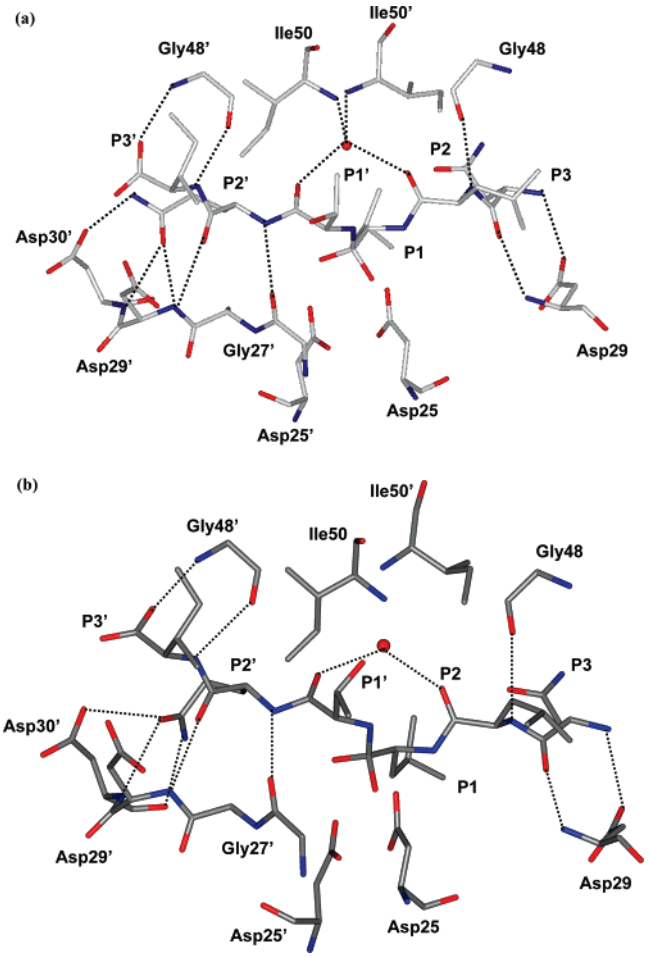

FIGURE 3: Hydrogen bond interactions of the tetrahedral intermediate with wild-type PR (a) and PR_{I54V} mutant (b) residues. Hydrogen bonds are indicated by dotted lines.

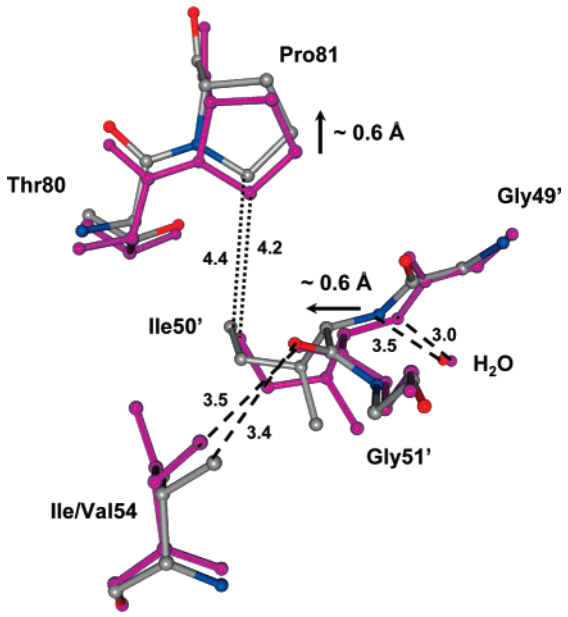

FIGURE 4: Superposition of PR_{WT}/TI (colored magenta) and PR_{I54V}/TI (colored by atom type) structures. The largest shifts occur for residues 50′ and 81 as indicated by arrows. The C−H···O contact of 3.5 Å between the main chain carbonyl of Ile50′ and the Cγ2 of Ile54 is maintained in the mutant structure, while the hydrophobic contacts of the Ile50′ side chain with Pro80 and the polar interaction of the Ile50′ amide with the water are elongated.

Pro81 by ~0.6 Å. In the other PR subunit, there is less change in the positions of the corresponding residues. Importantly, Ile54′ has no C−H···O interaction with the carbonyl of Ile50 because the latter is involved in the dimer-stabilizing hydrogen bond with the amide of Gly51′. Although Ile50 is shifted by ~0.6 Å from its position in the wild-type PR structure, it preserves van der Waals interactions with the mutated Val54′ and Pro81′. As a result, Pro81′ and Val82′ have no significant changes in their positions relative to those in the wild-type complex.

The PR_{I54V}/TI structure shows a small opening of the flaps around Ile50 and Ile50′ relative to those of the wild-type complex and coincident with the loss of interactions with the flap water. The weaker interaction of Ile50 and Ile50′ with peptide in the PR_{I54V}/TI complex is unusual, although an asymmetrical opening of one flap was observed in the structure of the inactive PR_{D25N} complex with a peptide (*39*). However, most crystal structures of PR single mutants with inhibitors, including peptide analogues, do not show such large changes in the flaps (*7*, *12*, *13*, *15*, *16*, *17*). Thus, it appears that the single non active site mutation I54V is capable of transmitting structural changes in a cascade of movements of PR residues that influence hydrogen bonds involved in stabilizing the substrate in the active site cavity.

Active Site Interactions in PR_{WT}/TI and Ligand-Free and Inhibitor-Bound PR Structures. The interactions of the catalytic Asp25 and Asp25′ in the PR/TI complex are critical for understanding the reaction mechanism. The most critical hydrogen bonds, and perhaps the most stabilizing, are between the two OH groups (OH_a and OH_b) of the central tetrahedral carbon of the TI and the carboxylate groups of Asp25 and Asp25′ (Figure 5). OH_a forms a very short hydrogen bond of 2.3 Å with the Oδ2 atom of Asp25′, whereas OH_b has two identical hydrogen bonds to Oδ1 and Oδ2 of Asp25 with a distance of 2.6 Å (distances are given between the heavy atoms). Additionally, OH_b is 3.2 Å away from the carboxylate oxygens of Asp25′. The nitrogen of the *gem*-diol−amine moiety of the TI is directed away from the Asp carboxylate groups. Its closest neighbor is Oδ2 of Asp25, which is 3.1 Å away. Similar interactions are found in the PR_{I54V}/TI structure, except that the OH_b is positioned 0.3 Å closer to the carboxylate oxygens of Asp25′.

The reaction mechanism can be discussed in relation to the crystal structures for the PR/TI (Figure 5a,b), unliganded PR (Figure 5c), and PR/inhibitor complexes. Recently, we reported the crystal structure of the unliganded HIV-1 PR with the flap mutation F53L at 1.35 Å resolution, which is the highest resolution attained for the unliganded PR (*40*). Although the mutation altered the interactions between the two flaps compared to those in the wild-type PR structure, no significant geometrical differences were observed for the active site residues Asp25 and Asp25′. Therefore, the unliganded PR_{F53L} structure will be used as a geometrical reference point for comparison of active site residues.

The unliganded PR is symmetric in the solid state; i.e., the two monomers have exactly the same geometry and are related by the crystallographic 2-fold axis. A water molecule is hydrogen-bonded to the catalytic aspartates and is equidistant from all four carboxylic oxygen atoms at 2.8 Å (Figure 5c). The inner carboxylate oxygen atoms of Asp25 and Asp25′ are 2.7 Å apart, while the planes of the carboxylates make a 46° dihedral angle. The catalytic Asp25

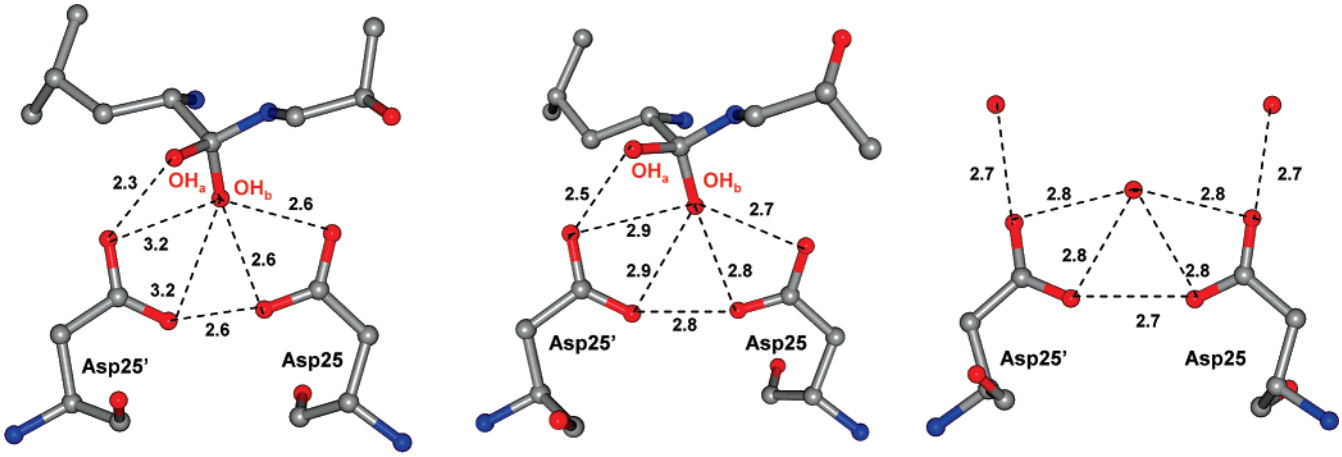

FIGURE 5: Hydrogen bonds in the active site of the (a) PR_{WT}/TI complex, (b) PR_{I54V}/TI complex, and (c) unliganded PR_{F53L} dimer. Only part of the TI molecule that includes residues Thr and Leu flanking the *gem*-diol moiety is shown in panels a and b for clarity.

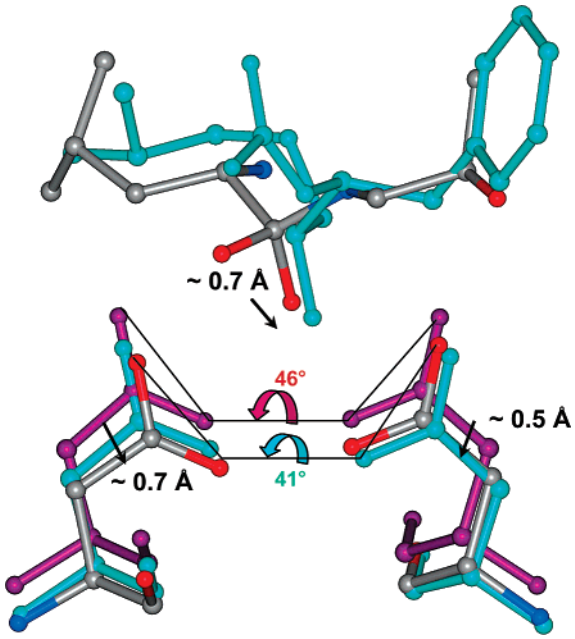

FIGURE 6: Superposition of active sites in PR_{F53L} (colored magenta), PR_{WT}/TI (colored by atom type), and PR_{WT}/DRV (colored cyan) structures. The shifts of Asp25, Asp25′, TI, and DRV relative to the unliganded structure are indicated by black arrows. The figure was created by aligning main chain atoms for the corresponding protein structures.

and Asp25′ have a different conformation in the unliganded PR structure than observed in the complexes with TI or inhibitor (Figure 6). Asp25 and Asp25′ shift significantly by 0.7−0.8 Å from their position in the unliganded structure to very similar positions when TI or inhibitor is bound in the structures of PR_{WT}/TI and PR/DRV. In the liganded structures the central OH group of DRV lies close to the site of OH_b of the TI; DRV mimics the mode of *gem*-diol coordination to the active site. The inner oxygen atoms of the catalytic aspartates have the same separation, while the dihedral angle between the COO planes decreases slightly to 41° in both PR_{WT}/TI and PR_{WT}/DRV structures. Therefore, the differences in active site geometry revealed in the ligand-free PR and PR/TI complex represent changes during different steps in the reaction mechanism.

DFT Calculations of the Positions of Hydrogen Atoms in the Active site and gem-Diol. To describe the reaction mechanism, it is essential to evaluate the positions of the hydrogen atoms, which are not determined experimentally in these crystal structures. Therefore, quantum chemical calculations were used to more accurately predict the positions of the critical hydrogen atoms. The positions of the hydrogen atoms in the active site were optimized for the ligand-free and TI-complexed PR structures. The initial peptide sequence with P1 Leu and P1′ Val was used for these calculations. In the former case, the positions of Asp25, Asp25′, and three water molecules were taken from the ligand-free PR_{F53L} structure. In the latter case, the positions of Asp25, Asp25′, a portion of TI (residues Val and Leu) surrounding the *gem*-diol, and the H_2O that links the TI with the flap amides were obtained from the current PR_{WT}/TI structure. Two different arrangements of hydrogen atom positions were considered: (1) a hydrogen atom is covalently bound to the inner oxygen of one of the Asp residues (Figure 7a,c); (2) a hydrogen atom is covalently bound to the outer oxygen of one of the Asp residues (Figure 7b,d). The active site was considered to be negatively charged in all the calculations, with one of the aspartic acids protonated and the other deprotonated.

The theoretical positions of the hydrogen atoms in the unliganded model are shown in Figure 7a,b. When the carboxylate H atom is placed on the inner oxygen, the central water molecule donates one hydrogen atom to make a hydrogen bond with the outer oxygen of the deprotonated carboxylate, while the other H atom has no interactions with the active site, and the OH bond is directed roughly perpendicular to the average plane of the carboxylates. Such an arrangement of the water H atoms allows the carboxylate hydrogen to contact both the central water (lytic water molecule) and the other carboxylate oxygen to form a bifurcated hydrogen bond. When the caboxylate is protonated to the outer oxygen atom, the lytic water rotates so that the HOH plane is almost parallel to the deprotonated COO^- moiety, allowing the formation of two hydrogen bonds (Figure 7b). In the *gem*-diol-bound active site, the OH groups of the intermediate interact with the outer oxygens of Asp25 and Asp25′ irrespective of the position of the active site proton, forming one very short hydrogen bond (Figure 7c,d). The corresponding H−O bond lengths are elongated to 1.03 Å, compared with 0.97 Å for the other OH group of the

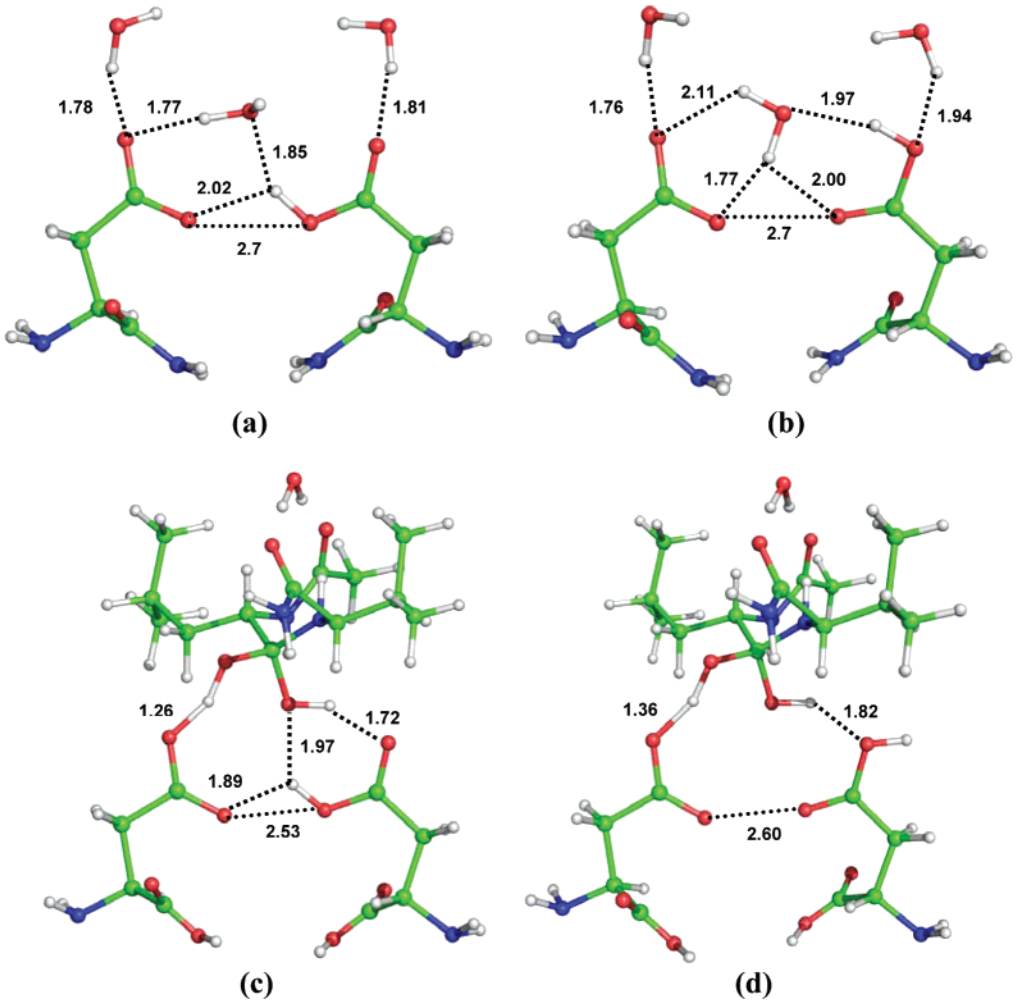

FIGURE 7: Positions of the hydrogen atoms in the active site of HIV-1 PR according to DFT calculations. The models with hydrogen on the inner carboxylate oxygen are stablized by 12 and 28 kcal/mol, respectively, for the ligand-free (a) and TI complex (c) relative to the alternate models (b, d).

tetrahedral carbon atom. The proton on the carboxylate oxygen forms a bifurcated hydrogen bond with the closest OH as discussed above for the unliganded active site. In the alternative model, the H atom bonded to the outer oxygen of Asp in the TI complex rotates away from the neighboring OH group of the TI to permit the formation of a hydrogen bond with the latter OH (Figure 7d).

Therefore, the models with the hydrogen atom placed on the inner, or the outer, oxygen of Asp25 show a substantial rearrangement of the other hydrogen positions in the active site. Interestingly, the active site is destabilized by ~12 and ~28 kcal/mol for the ligand-free (Figure 7b) and TI complex (Figure 7d) models, respectively, when the active site hydrogen is placed on the outer Asp oxygen. Such large amounts of energy cannot be supplied by thermal motion alone (kT = 0.6 kcal/mol, where k is the Boltzmann constant), and the more stable species will prevail in the solution at room temperature. Therefore, the quantum calculations are consistent with the hydrogen atom positioned on the inner carboxylate oxygen.

Mechanism of the Peptide Bond Cleavage Catalyzed by PR. We propose a modified mechanism of the peptide bond cleavage by HIV-1 PR based on the new structure of PR_{WT} complexed with the *gem*-diol intermediate and the previously determined unliganded PR_{F53L} structure (*40*). In the proposed mechanism of the hydrolysis reaction the initial geometry of the active site is similar to that found in the unliganded PR_{F53L}. The PR_{F53L} structure was selected as a starting point because it was refined with water molecules at a high resolution of 1.35 Å, while the other reported unliganded wild-type PR structures (*41*−*43*) are at lower resolution and lack water molecules. In the starting model the lytic water molecule is located above the side chains of Asp25 and Asp25′ and is equidistant from their outer oxygen atoms (Figure 8). In the active site the inner carboxylate oxygen atom of Asp25 is protonated with a hydrogen bond to the inner oxygen of Asp25′, while Asp25′ is deprotonated and therefore has a negative charge delocalized over its carboxylate group. Recent QM/MM calculations (*44*) using the B3LYP/6-311G+** DFT level of theory to model the active site residues have demonstrated that the former hydrogen bond represents a low-barrier hydrogen bond (LBHB; *45*). The hydrogen atom can move almost freely between the two Oδ2 atoms with the energy barrier estimated to be only ~1 kcal/mol. In such an arrangement the water is well situated to attack an incoming peptide bond (Figure 8, step A). The water attack on the peptide bond proceeds through a high-energy transition state (TS; step B) to the metastable intermediate structure in which the peptide group has been transformed into the *gem*-diol−amine moiety containing a

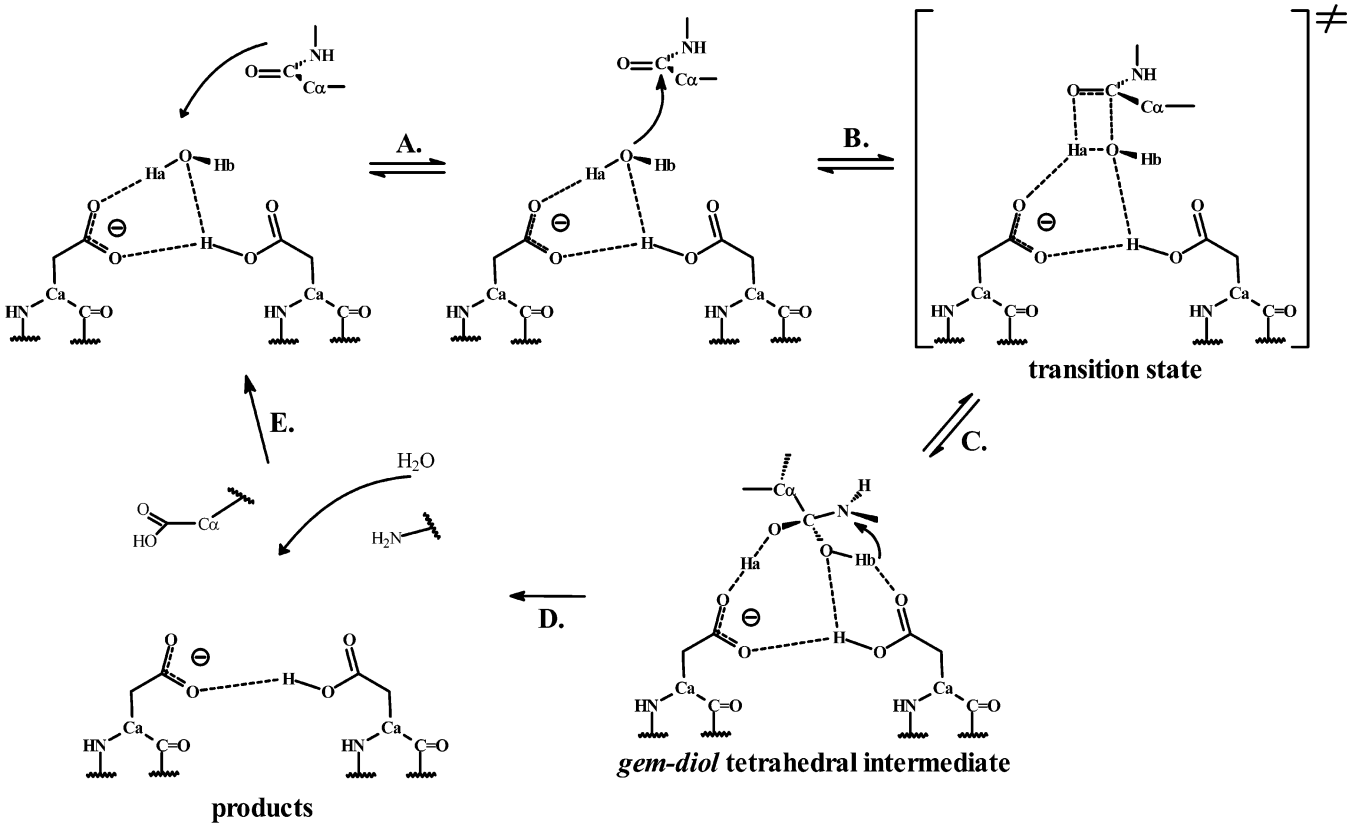

FIGURE 8: Proposed reaction mechanism of peptide bond hydrolysis by HIV-1 PR.

tetrahedral carbon atom (step C). The geometry of the TI is consistent with the experimentally observed positions of the OH groups relative to the active site aspartates (Figure 7). Although the hydrogen bond distances between the *gem*-diol and aspartates differ slightly in the PR_{WT}/TI and PR_{I54V}/TI structures, their overall arrangement remains very similar. The next step in the hydrolysis reaction is a proton transfer of H_b to the amine nitrogen of the TI (step D). Since the TI structure is greatly stabilized by the above-mentioned hydrogen bonds, the nitrogen protonation is expected to be a rate-determining step, similar to the proposal of Okimoto et al. (*22*). The resulting zwitterionic intermediate quickly decomposes to the products. The PR returns to its initial state by capturing a water molecule in the active site (step E). Hence, PR acts by activating the lytic water molecule and stabilizing the TS and TI structures by means of hydrogen bonding before returning to its starting geometry.

DISCUSSION

These new high-resolution crystal structures show the *gem*-diol TI of the peptide NLLTQI bound in the active site cavity of PR. HIV-1 PR can cleave substrates with a variety of sequences and with a minimal length of six residues (*46*). However, the PR activity will depend on the particular peptide sequence, especially at positions P1 and P1′ flanking the hydrolyzable peptide bond (*47*). The substitution of a single amino acid, such as a β-branched amino acid in the P1′ position, e.g., Val and Thr, can greatly diminish the ability of PR to hydrolyze the peptide (*48*). The peptide in this study (NLLTQI) has P1′ Thr and is expected to have very slow hydrolysis by PR. However, the hydrolysis reaction can proceed over the time scale of days that is necessary for crystal growth. Therefore, the presence of the tetrahedral intermediate in the crystal suggests that the TI decomposition into products is the rate-limiting step of this substrate hydrolysis, in agreement with kinetic studies of the reaction mechanism (*49*, *50*).

The *gem*-diol−amine tetrahedral intermediate of the substrate binds in the active site cavity in the extended conformation and forms a number of hydrogen bonds with PR residues (Figure 3), similar to the mode of binding seen in PR/substrate analogue complexes (*12*). The *gem*-diol hydroxyl OH_a has a very strong hydrogen bond with the outer oxygen atom of Asp25′ of 2.3 and 2.5 Å length in the wild-type PR and I54V mutant structures, respectively, and makes no close contacts with the other aspartic acid. On the other hand, OH_b interacts more closely with Asp25. According to the theoretical calculations, the OH_b substituent is bidentate: it donates its hydrogen to make the hydrogen bond with the outer oxygen and accepts a hydrogen bond from the protonated inner oxygen of Asp25 (Figure 7c). Additionally, the protonated inner oxygen of Asp25 has a bifurcated hydrogen bond. The hydrogen atom is donated to make interactions with the OH_b group and with the inner oxygen of Asp25′. The I54V mutation of PR, which introduces the sterically smaller Val side chain, does not disrupt the direct hydrogen bonds between PR_{I54V} and TI. However, the water-mediated interactions with the flap residues Ile50 and Ile50′ have been lost. The flap water is shifted by 0.2 Å from its position in the wild-type structure, which, together with the ~0.5 Å movements of Ile50 and Ile50′, eliminates two of the four hydrogen bonds usually observed for the flap water molecule in many PR/ligand complexes (*7*, *11*, *13*, *15*, *16*, *17*, *27*). The loss of these hydrogen bonds has not been observed previously in peptide complexes with drug-resistant mutants. It implies a more loosely bound substrate and lower

catalytic activity for this PR_{I54V} mutant, which may provide the mechanism for drug resistance. Hence, these two new structures have provided evidence for the geometry of the TI of the PR-catalyzed hydrolysis reaction, as well as revealed differences in substrate binding of the drug-resistant mutant.

The specific pathway of how PR hydrolyzes the peptide bond has been hotly debated for over 15 years, with a number of groups studying the mechanism experimentally and/or theoretically. The generally accepted mechanism involves a metastable *gem*-diol intermediate as confirmed by ^{18}O-exchange NMR experiments (*19*, *49*, *50*). Although there is a consensus in the description of the HIV-1 PR active site as a negatively charged Asp25−Asp25′ dyad, no agreement has been reached on the exact position of the proton. Theoretically, this proton can be placed on either an inner or an outer carboxylate oxygen atom of Asp25 or Asp25′. In all available PR structures (inhibited or unliganded) the inner oxygen atoms of Asp25 and Asp25′ are quite close to each other (∼2.5−2.7 Å), suggesting that the proton resides on an inner oxygen. Such a protonation state produces a strong hydrogen bond and minimizes destabilizing charge−charge interactions between the two partially negative oxygen atoms. However, the outer oxygen is protonated in a number of theoretical calculations of the mechanism. The modeled reaction proceeds by a two-hydrogen transfer to generate the intermediate (*20*−*22*). In the calculations the proton bonded to the outer oxygen of Asp25 attacks the peptide bond oxygen, while the lytic water attacks the peptide bond carbon and, subsequently, transfers its hydrogen to Asp25′. This process generates a neutral tetrahedral intermediate and switches the protonation states of Asp25 and Asp25′. The reaction proceeds to transfer a proton from Asp25′ to the peptide nitrogen, producing a second tetrahedral intermediate, which then degrades to the products. In different calculations one of the OH groups of the TI was positioned either right between the inner oxygens of the two aspartates (*20*) or as far away as 3.3 Å from even the outer oxygens (*51*). Only in two theoretical studies has a mechanism involving protonation of the inner oxygen of Asp25 been proposed (*23*, *24*). In these QM/MM molecular dynamics simulations the lytic water molecule donates its proton to Asp25′. As a consequence, a neutral active site is generated, leaving the *gem*-diol intermediate negatively charged. In this *gem*-diol the negatively charged oxygen has no contacts with the aspartates.

The theoretical tetrahedral intermediate geometries described above clearly disagree with the PR_{WT}/TI structure studied here, in which both OH groups of the TI have strong hydrogen bonds with the active site residues. Therefore, we have proposed a modified mechanism of the peptide bond cleavage by HIV-1 PR, which is based on the unliganded PR_{F53L} structure (*40*) representing the initial geometry and the new structure of PR_{WT} complexed with the *gem*-diol intermediate representing the TI. Moreover, it is consistent with the reported structures of a disordered TI complex (*25*) and a product complex (*52*) and the monoprotonation of the catalytic aspartates (the pK_a values are ∼2.5 and ∼6.2 (*53*)). The inner oxygen atom of Asp25 is protonated, in agreement with the observed geometry in the PR_{WT}/TI structure. In this mechanism the PR acts by activating the lytic water molecule, stabilizing the TS and TI structures, and remains intact while returning to its starting geometry (Figure 8). During the reaction the PR makes no covalent bonds and does not transfer its own H atoms to the reactants.

In conclusion, we have trapped a high-energy intermediate state along the path of PR-catalyzed peptide hydrolysis reaction in the wild-type and I54V mutant enzymes. The structural changes caused by the single mutation suggest that substrate binds more weakly in the PR_{I54V} complex, which may contribute to drug resistance. On the basis of the current PR_{WT}/TI structure and our previous structure of the unliganded PR_{F53L}, we proposed a modified mechanism of the peptide cleavage reaction in which no hydrogen atoms are transferred from the PR. Quantum chemical calculations demonstrated that the protonation of the inner carboxylic oxygen of catalytic Asp stabilized the active site, whereas the placement of the hydrogen on the outer oxygen of Asp destabilized the structure significantly. However, the actual positions of the H atoms in PR still remain to be defined experimentally.

ACKNOWLEDGMENT

We are grateful to Jane M. Sayer and Brian M. Martin for their help to resolve the ambiguities of the crystal complexes by mass spectrometry and N-terminal protein sequencing and to Robert W. Harrison and Yunfeng Tie for valuable discussion and assistance with refinement. We thank the staff at the SER-CAT beamline at the Advanced Photon Source, Argonne National Laboratory, for assistance during X-ray data collection. We thank the staff at the Georgia State University computer center for help with setting up GAUSSIAN on the IBM System p5 575 supercomputer.

REFERENCES

1. Emini, E. A. (2002) *The Human Immunodeficiency Virus: Biology, Immunology, and Therapy*, 523 pp, Princeton University Press, Princeton, NJ.
2. Ogden, R. (2003) HIV Protease Inhibitors, *Infect. Dis. Ther. 30*, 523−553.
3. Marks, K., and Gulick, R. M. (2005) Progress in HIV Treatment, *HIV Chemother.*, 1−32.
4. Johnson, V. A., Brun-Vezinet, F., Clotet, B., Kuritzkes, D. R., Pillay, D., Schapiro, J. M., and Richman, D. D. (2006) Update of the Drug Resistance Mutations in HIV-1: Fall 2006, *Top. HIV Med. 14*, 125−130.
5. Foulkes, J. E., Prabu-Jeyabalan, M., Cooper, D., Henderson, G. J., Harris, J., Swanstrom, R., and Schiffer, C. A. (2006) Role of Invariant Thr80 in Human Immunodeficiency Virus Type 1 Protease Structure, Function, and Viral Infectivity, *J. Virol. 80*, 6906−6916.
6. Heaslet, H., Kutilek, V., Morris, G. M., Lin, Y.-C., Elder, J. H., Torbett, B. E., and Stout, C. D. (2006) Structural Insights into the Mechanisms of Drug Resistance in HIV-1 Protease NL4-3, *J. Mol. Biol. 356*, 967−981.
7. Kovalevsky, A. Y., Tie, Y., Liu, F., Boross, P. I., Wang, Y.-F., Leshchenko, S., Ghosh, A. K., Harrison, R. W., and Weber, I. T. (2006) Effectiveness of Nonpeptide Clinical Inhibitor TMC-114 on HIV-1 Protease with Highly Drug Resistant Mutations D30N, I50V, and L90M, *J. Med. Chem. 49*, 1379−1387.
8. Clemente, J. C., Moose, R. E., Hemrajani, R., Whitford, L. R. S., Govindasamy, L., Reutzel, R., McKenna, R., Agbandje-McKenna, M., Goodenow, M. M., and Dunn, B. M. (2004) Comparing the Accumulation of Active- and Nonactive-Site Mutations in the HIV-1 Protease, *Biochemistry 43*, 12141−12151.
9. Hong, L., Zhang, X. C., Hartsuck, J. A., and Tang, J. (2000) Crystal Structure of an In Vivo HIV-1 Protease Mutant in Complex with Saquinavir: Insights into the Mechanisms of Drug Resistance, *Protein Sci. 9*, 1898−1904.
10. King, N. M., Prabu-Jeyabalan, M., Nalivaika, E. A., Wigerinck, P., de Bethune, M.-P., and Schiffer, C. (2004) Structural and

Thermodynamic Basis for the Binding of TMC114, a Next-Generation Human Immunodeficiency Virus Type 1 Protease Inhibitor, *J. Virol. 78*, 12012−12021.
11. Liu, F., Boross, P. I., Wang, Y.-F., Tozser, J., Louis, J. M., Harrison, R. W., and Weber, I. T. (2005) Kinetic, Stability, and Structural Changes in High-resolution Crystal Structures of HIV-1 Protease with Drug-resistant Mutations L24I, I50V, and G73S, *J. Mol. Biol. 354*, 789−800.
12. Tie, Y., Boross, P. I., Wang, Y.-F., Gaddis, L., Liu, F., Chen, X., Tozser, J., Harrison, R. W., and Weber, I. T. (2005) Molecular Basis for Substrate Recognition and Drug Resistance from 1.1 to 1.6 Å Resolution Crystal Structures of HIV-1 Protease Mutants with Substrate Analogs, *FEBS J. 272*, 5265−5277.
13. Mahalingam, B., Louis, J. M., Hung, J., Harrison, R. W., and Weber, I. T. (2001) Structural Implications of Drug-Resistant Mutants of HIV-1 Protease: High-Resolution Crystal Structures of the Mutant Protease/Substrate Analogue Complexes, *Proteins: Struct., Funct., Genet. 43*, 455−464.
14. Mahalingam, B., Boross, P. I., Wang, Y.-F., Louis, J. M., Fischer, C. C., Tozser, J., Harrison, R. W., and Weber, I. T. (2002) Combining Mutations in HIV-1 Protease to Understand Mechanisms of Resistance, *Proteins: Struct., Funct., Genet. 48*, 107−116.
15. Prabu-Jeyabalan, M., Nalivaika, E. A., and Schiffer, C. (2002) Substrate Shape Determines Specificity of Recognition for HIV-1 Protease: Analysis of Crystal Structures of Six Substrate Complexes, *Structure 10*, 369−381.
16. Prabu-Jeyabalan, M., Nalivaika, E. A., and Schiffer, C. (2000) How Does a Symmetric Dimer Recognize an Asymmetric Substrate? A Substrate Complex of HIV-1 Protease, *J. Mol. Biol. 301*, 1207−1220.
17. Prabu-Jeyabalan, M., Nalivaika, E. A., Schiffer, C., and King, N. M. (2003) Viability of a Drug-Resistant Human Immunodeficiency Virus Type 1 Protease Variant: Structural Insights for Better Antiviral Therapy, *J. Virol. 77*, 1306−1315.
18. Brik, A., and Wong, C.-H. (2003) HIV-1 Protease: Mechanism and Drug Discovery, *Org. Biomol. Chem. 1*, 5−14.
19. Hyland, L. J., Tomaszek, T. A., Jr., and Meek, T. D. (1991) Human Immunodeficiency Virus-1 Protease. 2. Use of pH Rate Studies and Solvent Kinetic Isotope Effects to Elucidate Details of Chemical Mechanism, *Biochemistry 30*, 8454−8463.
20. Liu, H., Müller-Plathe, F., and van Gunsteren, W. F. (1996) A combined Quantum/Classical Molecular Dynamics Study of the Catalytic Mechanism of HIV Protease, *J. Mol. Biol. 261*, 454−469.
21. Chatfield, D. C., Eurenius, K. P., and Brooks, B. R. (1998) HIV-1 Protease Cleavage Mechanism: A Theoretical Investigation Based on Classical MD Simulation and Reaction Path Calculations Using a Hybrid QM/MM Potential, *J. Mol. Struct. 423*, 79−92.
22. Okimoto, N., Tsukui, T., Hata, M., Hoshino, T., and Tsuda, M. (1999) Hydrolysis Mechanism of the Phenylalanine-Proline Peptide Bond Specific to HIV-1 Protease: Investigation by the ab initio Molecular Orbital Method, *J. Am. Chem. Soc. 121*, 7349−7354.
23. Trylska, J., Grochowski, P., and McCammon, J. A. (2004) The Role of Hydrogen Bonding in the Enzymatic Reaction Catalyzed by HIV-1 Protease, *Protein Sci. 13*, 513−528.
24. Piana, S., Bucher, D., Carloni, P., and Rothlisberger, U. (2004) Reaction Mechanism of HIV-1 Protease by Hybrid Car-Parrinello/Classical MD Simulations, *J. Phys. Chem. 108*, 11139−11149.
25. Kumar, M., Prashar, V., Mahale, S., and Hosur, M. V. (2005) Observation of a Tetrahedral Reaction Intermediate in the HIV-1 Protease-Substrate Complex, *Biochem. J. 389*, 365−371.
26. Louis, J. M., Clore, G. M., and Gronenborn, A. M. (1999) Autoprocessing of HIV-1 Protease Is Tightly Coupled to Protein Folding, *Nat. Struct. Biol. 6*, 868−875.
27. Mahalingam, B., Louis, J. M., Reed, C. C., Adomat, J. M., Krouse, J., Wang, Y.-F., et al. (1999) Structural and Kinetic Analysis of Drug Resistant Mutants of HIV-1 Protease, *Eur. J. Biochem. 263*, 238−245.
28. Otwinowski, Z., and Minor, W. (1997) Processing of X-ray Diffraction Data in Oscillation Mode, *Methods Enzymol. 276*, 307−326.
29. Collaborative Computational Project, Number 4. (1994) The CCP4 Suite: Programs for Protein Crystallography, *Acta Crystallogr., Sect. D 50*, 760−763.
30. Potterton, E., Briggs, P., Turkenburg, M., and Dodson, E. A. (2003) Graphical User Interface to the CCP4 Program Suite, *Acta Crystallogr., Sect. D 59*, 1131−1137.
31. Tie, Y., Boross, P., Wang, Y.-F., Gaddis, L., Hussain, A. K., Leshchenko, S., et al. (2004) High Resolution Crystal Structures of HIV-1 Protease with a Potent Nonpeptide Inhibitor (UIC-94017) Active against Multidrug-Resistant Clinical Strains, *J. Mol. Biol. 338*, 341−352.
32. Sheldrick, G. M., and Schneider, T. R. (1997) High Resolution Refinement, *Methods Enzymol. 277*, 319−343.
33. Jones, T. A., Zou, J. Y., Cowan, S. W., and Kjeldgaard, M. (1991) Improved Methods for Building Protein Models in Electron Density Maps and the Location of Errors in These Models, *Acta Crystallogr., Sect. A 47*, 110−119.
34. DeLano, W. L. (2002) *The PyMOL Molecular Graphics System*, DeLano Scientific, San Carlos, CA.
35. Frisch, M. J., Trucks, G. W., Schlegel, H. B., Scuseria, G. E., Robb, M. A., Cheeseman, J. R., Montgomery, J. A., Jr., Vreven, T., Kudin, K. N., Burant, J. C., Millam, J. M., Iyengar, S. S., Tomasi, J., Barone, V., Mennucci, B., Cossi, M., Scalmani, G., Rega, N., Petersson, G. A., Nakatsuji, H., Hada, M., Ehara, M., Toyota, K., Fukuda, R., Hasegawa, J., Ishida, M., Nakajima, T., Honda, Y., Kitao, O., Nakai, H., Klene, M., Li, X., Knox, J. E., Hratchian, H. P., Cross, J. B., Bakken, V., Adamo, C., Jaramillo, J., Gomperts, R., Stratmann, R. E., Yazyev, O., Austin, A. J., Cammi, R., Pomelli, C., Ochterski, J. W., Ayala, P. Y., Morokuma, K., Voth, G. A., Salvador, P., Dannenberg, J. J., Zakrzewski, V. G., Dapprich, S., Daniels, A. D., Strain, M. C., Farkas, O., Malick, D. K., Rabuck, A. D., Raghavachari, K., Foresman, J. B., Ortiz, J. V., Cui, Q., Baboul, A. G., Clifford, S., Cioslowski, J., Stefanov, B. B., Liu, G., Liashenko, A., Piskorz, P., Komaromi, I., Martin, R. L., Fox, D. J., Keith, T., Al-Laham, M. A., Peng, C. Y., Nanayakkara, A., Challacombe, M., Gill, P. M. W., Johnson, B., Chen, W., Wong, M. W., Gonzalez, C., and Pople, J. A. (2004) *Gaussian 03*, revision C.02, Gaussian, Inc., Wallingford, CT.
36. Mildner, A. M., Rothrock, D. J., Leone, J. W., Bannow, C. A., Lull, J. M., Reardon, I. M., Sarcich, J. L., Howe, W. J., Tomich, C. S., Smith, C. W., et al. (1994) The HIV-1 Protease as Enzyme, and Substrate: Mutagenesis of Autolysis Sites, and Generation of a Stable Mutant with Retained Kinetic Properties, *Biochemistry 33*, 9405−13.
37. Tozser, J., Bagossi, J., Weber, I. T., Copeland, T. D., and Oroszlan, S. (1996) Comparative Studies on the Substrate Specificities of Avian Myeloblastosis Virus Proteinase and Lentivirus Proteinases, *J. Biol. Chem. 271*, 6781−6788.
38. Weber, I. T., Wu, J., Adomat, J., Harrison, R. W., Kimmel, A. R., Wondrak, E. M., and Louis, J. M (1997) Crystallographic Analysis of Human Immunodeficiency Virus Type 1 Protease with an Analog of the Conserved CA-p2 substrate. Interactions with Frequently Occurring Glutamic Acid Residue at P2′ Position of Substrates, *Eur. J. Biochem. 249*, 523−530.
39. Prabu-Jeyabalan, M., Nalivaika, E. A., Romano, K., and Schiffer, C. A (2006) Mechanism of Substrate Recognition by Drug-Resistant Human Immunodeficiency Virus Type 1 Protease Variants Revealed by a Novel Structural Intermediate, *J. Virol. 80*, 3607−3616.
40. Liu, F., Kovalevsky, A. Y., Louis, J. M., Boross, P. I., Wang, Y.-F., Harrison, R. W., and Weber, I. T. (2006) Mechanism of Drug Resistance Revealed by the Crystal Structure of the Unliganded HIV-1 Protease with F53L Mutation, *J. Mol. Biol. 358*, 1191−1199.
41. Spinelli, S., Liu, Q. Z., Alzari, P. M., Hirel, P. H., and Poljak, R. J. (1991) The Three-Dimensional Structure of the Aspartyl Protease from the HIV-1 Isolate BRU, *Biochimie 73*, 1391−1395.
42. Lapatto, R., Blundell, T., Hemmings, A., Overington, J., Wilderspin, A., and Wood, S. (1989). X-ray Analysis of HIV-1 Proteinase at 2.7 Å Resolution Confirms Structural Homology among Retroviral Enzymes, *Nature 342*, 299−302.
43. Wlodawer, A., Miller, M., Jaskolski, M., Sathyanarayana, B. K., Baldwin, E., Weber, I. T. (1989). Conserved Folding in Retroviral Proteases: Crystal Structure of a Synthetic HIV-1 Protease, *Science 245*, 616−621.
44. Porter, M. A., and Molina, P. A. (2006) The Low-Barrier Double-Well Potential of the $O^{\delta 1}$-H-$O^{\delta 1}$ Hydrogen Bond in Unbound HIV Protease: A QM/MM Characterization, *J. Chem. Theory Comput.* (in press).
45. Grabowski, S. J. (2006) Theoretical Studies of Strong Hydrogen Bonds, *Annu. Rep. Prog. Chem., Sect. C 102*, 131−165.
46. Pettit, S. C., Michael, S. F., and Swanstrom, R. (1993) The specificity of the HIV-1 protease, *Perspect. Drug Discovery Des. 1*, 69−83.

47. Louis, J. M., Weber, I. T., Tozser, J., Clore, G. M., and Gronenborn, A. M. (2000) HIV-1 Protease: Maturation, Enzyme Specificity, and Drug Resistance, *Adv. Pharmacol. 49*, 111−146.
48. Phylip, L. H., Richards, A. D., Kay, J., Konvalinka, J., Strop, P., Blaha, I., Velek, J., Kostka, V., Ritchie, A. J., Broadhurst, A. V., Farmerie, W. G., Scarborough, P. E., and Dunn, B. M. (1990) Hydrolysis of Synthetic Chromogenic Substrates by HIV-1 and HIV-2 Proteinases, *Biochem. Biophys. Res. Commun. 171*, 439−444.
49. Polgar, L., Szeltner, Z., and Boros, I. (1994) Substrate-Dependent Mechanisms in the Catalysis of Human Immunodeficiency Virus Protease, *Biochemistry 33*, 9351−9357.
50. Hyland, L. J., Tomaszek, T. A., Jr., Roberts, G. D., Carr, S. A., Magaard, V. W., Bryan, H. L., Fakhoury, S. A., Moore, M. L., Minnich, M. D., Culp, J. S., DesJarlais, R. L., and Meek, T. D. (1991) Human Immunodeficiency Virus-1 Protease. 1. Initial Velocity Studies and Kinetic Characterization of Reaction Intermediates by ^{18}O Isotope Exchange, *Biochemistry 30*, 8441−8453.
51. Chatfield, D. C., and Brooks, B. R. (1995) HIV-1 Protease Cleavage Mechanism Elucidated with Molecular Dynamics Simulation, *J. Am. Chem. Soc. 117*, 5561−5572.
52. Das, A., Prashar, V., Mahale, S., Serre, L., Ferrer, J.-L., and Hosur, M. V. (2006) Crystal Structure of HIV-1 Protease in situ Product Complex and Observation of a Low-Barrier Hydrogen Bond Between Catalytic Aspartates, *Proc. Natl. Acad. Sci. U.S.A. 103*, 18464−18469.
53. (53) Wang, Y. X., Freedberg, D. I., Yamazaki, T., Wingfield, P. T., Stabl, S. J., Kaufman, J. D., Kiso, Y., and Torchia, D. A. (1996) Solution NMR Evidence That HIV-1 Protease Catalytic Aspartyl Groups Have Different Ionization States in the Complex formed with the Asymmetric Drug KNI-272, *Biochemistry 35*, 9945−9950.

BI700822G